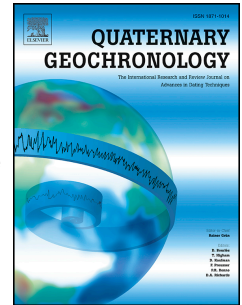


Accepted Manuscript

Identifying chronostratigraphic breaks in aeolian sediment profiles using near-surface luminescence dating and changepoint analysis

Catherine E. Buckland, Richard M. Bailey, David S.G. Thomas



PII: S1871-1014(17)30186-3

DOI: [10.1016/j.quageo.2018.03.011](https://doi.org/10.1016/j.quageo.2018.03.011)

Reference: QUAGEO 909

To appear in: *Quaternary Geochronology*

Received Date: 27 November 2017

Revised Date: 22 March 2018

Accepted Date: 22 March 2018

Please cite this article as: Buckland, C.E., Bailey, R.M., Thomas, D.S.G., Identifying chronostratigraphic breaks in aeolian sediment profiles using near-surface luminescence dating and changepoint analysis, *Quaternary Geochronology* (2018), doi: 10.1016/j.quageo.2018.03.011.

This is a PDF file of an unedited manuscript that has been accepted for publication. As a service to our customers we are providing this early version of the manuscript. The manuscript will undergo copyediting, typesetting, and review of the resulting proof before it is published in its final form. Please note that during the production process errors may be discovered which could affect the content, and all legal disclaimers that apply to the journal pertain.

Identifying chronostratigraphic breaks in aeolian sediment profiles using near-surface luminescence dating and changepoint analysis.

Catherine E. Buckland*, Richard M. Bailey, David S. G. Thomas

School of Geography and the Environment, University of Oxford, South Parks Road, Oxford, OX1 3QY

* Corresponding author

E-mail address: catherine.buckland@ouce.ox.ac.uk (Catherine E. Buckland)

Keywords

changepoint

chronostratigraphy

aeolian systems

environmental noise

luminescence dating

thresholds

Abstract

Optical dating of depositional profiles provides information on environmental change and dune reactivation in aeolian systems. However, identifying the optimum locations and samples for luminescence dating is often confounded by a lack of visible internal structures and a highly discontinuous and heterogeneous record. We use a method that combines high-resolution coarse luminescence signals with statistical changepoint analysis to identify significant chronostratigraphic breaks. The changepoint algorithm demonstrates an ability to identify changes in a depositional profile with depth, allowing luminescence dating to be better-focused on specific points of chronological change. Likewise, this method ensures that chronostratigraphical breaks in the record are not missed due to coarse sampling strategies. This method is applied to a dataset from near-surface dune profiles from the Nebraska Sandhills, testing whether fully-prepped SAR luminescence ages from an identified chronostratigraphic section are representative of the wider unit identified in the changepoint analysis. Unlike previous methods, this therefore ensures that resultant chronologies are a factor of true chronological breaks as opposed to aliasing (i.e. misidentification of a signal), and capture the heterogeneous record across the dynamic environment.

1. Introduction

Depositional records in aeolian systems provide information on environmental change over Quaternary timescales. Robust high-resolution chronologies of depositional events are a fundamental part of reconstructing past aeolian systems dynamics and testing geomorphological hypotheses. Optically stimulated luminescence (OSL) dating techniques provide an excellent method of dating depositional records and reconstructing environmental history, providing time-series of deposition and activation events in an environment relatively starved of alternative proxies (Thomas and Burrough, 2012).

However, identifying appropriate locations for OSL sampling is difficult for two main reasons. First, selecting the most appropriate locations to extract sediment samples is often hampered by high levels of “environmental noise” in aeolian sedimentary systems. Aeolian systems can have spatially inconsistent records due to localised variability in the processes that induce accumulation and erosion (Telfer et al., 2010, 2017; Leighton et al., 2014; Thomas and Burrough, 2013; Stone and Thomas, 2008; Telfer and Thomas, 2007; Munyikwa, 2005) including wind energy (Fryberger, 1979), sediment moisture content, vegetation cover (Wolfe and Nickling, 1993) and sediment availability (Kocurek and Lancaster, 1999). Thus, aeolian records are inherently discontinuous and this can be problematic when, for example, attempting to establish the history of dune accumulation and its relationship to climatic and environmental changes; a problem often compounded by a sampling strategy relying upon relatively few samples (Telfer et al., 2010; Stone and Thomas, 2008). Individual chronological profiles from a feature reflect the localised response to a suite of disturbances (Leighton et al., 2014), and are not necessarily representative of the wider landscape (or landform) response. Bailey and Thomas (2014) explore this with a quantitative model in which a series of ‘filters’ demonstrate how information on past forcing conditions is progressively lost from the stratigraphic record and a discontinuous sequence is produced. With a range of disturbance factors occurring at a series of spatial scales, sampling strategies which seek to understand aeolian geomorphological development need a method which averages out the environmental noise and identifies a true landscape response which captures the structure of the depositional profile whilst acknowledging the incomplete nature of the record (Thomas and Bailey, 2017). An accurate interpretation of aeolian geomorphological features (e.g. dune records) requires an improved understanding of how the luminescence ages relate to the sediments that have been preserved within the feature (Thomas, 2013; Lomax et al., 2011; Chase, 2009; Stone and Thomas, 2008; Munyikwa,

2005). Choosing the exact point at which to sample a chosen landscape or landform to build a profile of the landscape response, however, is a complex process.

Second, while lithostratigraphy and sedimentary structures can sometimes provide information in the field to guide sampling strategy (e.g. Atkinson et al., 2011; Fitzsimmons and Telfer, 2008; Fitzsimmons et al., 2007), visible structures are widely absent, and even if present, sampling strategies (e.g. vertical drilling) can make them invisible. In these contexts, it is not possible to visually identify optimal places to sample for dating. As Leighton et al. (2013) discuss, if the internal structure and bounding surfaces of dunes are not visible, the resultant chronology is at risk of being determined by sampling resolution as opposed to depositional structure within the feature. Hence, there is a need to ascertain a method which can identify chronostratigraphical breaks in the record which were perhaps not long enough to allow the development of other boundaries (e.g. pedogenesis). A homogenous section may have accumulated gradually over time, or in an individual depositional event; yet it may also be the result of a series of short-lived sporadic and pulsed depositional events. Where distinctive lithological variations are not visible, the development of a high-resolution chronology is key to identifying the distinctive breaks in the record and assessing how the climatostratigraphy compares with the chronostratigraphy in the absence of lithostratigraphy (Leighton et al., 2014; Stevens et al., 2006).

Sampling at only two points within a profile and extrapolating the age-depth relationship might be suitable in locations where a linear relationship exists between accumulation and depth and the site has experienced quasi-continuous deposition over time (Figure 1a). However, in aeolian systems we would not expect to find quasi-continuous accumulation; a pulsed depositional profile is far more likely for two reasons. Firstly, aeolian system sedimentary profiles are constructed because a series of accumulation and erosion events create discontinuous deposited profiles (Bateman et al., 2017; Bailey and Thomas, 2014; Singhvi and Porat, 2008; Stone and Thomas, 2008; Telfer and Thomas, 2007). Secondly, the process of deposition is discontinuous in aeolian systems (i.e. at seconds, inter-seasonal, inter-annual, and timescales up to inter-millennial), and where there is a lack of visible stratigraphic or sedimentological variability, sampling will likely miss locations where chronostratigraphic breaks occur; losing an understanding of the overall depositional structure due to under-sampling. Understanding the depositional structure of the sedimentary profile is the key to deciphering potential hiatuses in the accumulation record, but also in highlighting sections where post-depositional erosion may have impacted on the preserved record (Hughes, 2010).

To capture the depositional variability of aeolian systems, several sediment samples (taken both vertically and horizontally) are needed for dating. In a system with significant levels of environmental noise, the only means to capture the complete signal is to increase sample numbers until a pattern can be identified amongst the noise. However, dating numerous sediments at a high-resolution is often not within the time and cost requirements of an individual project, and may prove futile if all the sediments in one feature are of the same age (i.e. within overlapping age errors). Equally, determining a threshold number of samples to extract is hard to define and equally variable between sites depending on the sedimentary characteristics and the research question being investigated. Therefore, a means of rapidly scanning the sedimentary section to understand the depositional structure prior to focusing full-preparation dating efforts is needed.

In settings where stratigraphical information is absent, portable luminescence readers and partial-preparation techniques have the potential to provide a rapid guide to sampling strategy. Portable luminescence readers have made some progress in devising a method for rapid relative age testing (e.g. Bateman et al., 2015; Stone et al., 2015; Sanderson and Murphy, 2010). However, portable luminescence studies are limited in the scale of sub-sampling resolution that they can provide across a feature and it is still necessary to select the points at which to measure the signal. Considering this, whilst providing a rapid age estimate, the interpretation of sediment accumulation records may be prone to aliasing; a function of the sample selection as opposed to genuine chronostratigraphic breaks in the sequence. Furthermore, portable luminescence measurements are not sensitivity-corrected and are thus susceptible to changes in sensitivity. For example, the luminescence variability reported between samples measured using a portable luminescence reader could be dependent on the volume of sediment which is being measured or the sensitivity of sediment to OSL, potentially masking subtle changes in the chronology of the sediments across a sequence.

Alternatively, many existing studies have produced rapid assessments of equivalent dose (D_e) and estimated ages using a variety of partial-preparation techniques (e.g. Leighton and Bailey, 2015; Durcan et al., 2010; Roberts et al., 2009) to eliminate additional steps in age estimate production. Nevertheless, applying partial-preparation techniques to a collection of samples still requires initial decision-making over which samples to measure. In addition, whilst not as lengthy as full-preparation procedures, completing partial-preparation and range-finder methods for numerous samples at a high-resolution is often outside the time capacity and resourcing of most research projects. Standardised Growth Curves (SGCs) have also been used to reduce the time required to produce age estimates (Munyikwa and Brown, 2014; Yang et al., 2011; Telfer et al., 2008; Roberts and Duller, 2004). However,

whilst reducing the time spent producing age estimates, the method does not provide any additional insight into the depositional structure of the sediments or highlight the optimal locations to deploy focus full-preparation dating to extract maximum chronological information. In the absence of a method which allows us to produce rapid luminescence results at a high-resolution, a landscape response will be subject to high levels of environmental noise.

As part of a wider investigation into the recent aeolian dynamics of the Nebraska Sandhills, a high-resolution chronology of activity was required to allow deposition events to be determined. This paper presents a method for the rapid testing of relative age variability to inform sample selection for full luminescence dating; an approach that focuses on intensive sampling of the depositional environment in the field and then subsequent rapid analysis to establish which samples best capture break points in accumulation. The premise is that it is necessary to allocate luminescence dating efforts, expensive in both time and money, as effectively as possible. This research presents an attempt to identify the specific sampling locations where the environmental and chronological information gained is of greatest value and best represents the history of accumulation and erosion.

This study uses L_x/T_x measurements (i.e. sensitivity-corrected natural luminescence signals) of un-prepared samples coupled with a statistical method (changepoint analysis) which identifies breaks in L_x/T_x -depth data to identify the depositional structure of near-surface sediments across a range of sand dunes and blowouts in the Nebraska Sandhills. L_x/T_x data is used to control for the effects of variation in aliquot mass and sample luminescence sensitivity (to dose) through the core. The noisy nature of a high-resolution bulk signal luminescence dataset requires a subsequent decision to be made about the structure of the depositional profile. This decision can be made qualitatively, identifying structures within the luminescence profile visually; however, this paper presents an algorithmic method through a statistical model. Using this approach, high-resolution age profiles are created which are used to identify step-changes in the record which can subsequently be used to focus full-preparation dating. Mid-point sub-samples from identified changepoint sections are dated using full-preparation methods and tested against fully-prepared ages from the corresponding sections to test the suitability of the method. In doing so, this paper aims to develop a method which can: improve stratigraphical understanding of aeolian features; identify optimum samples for luminescence dating; capture an environmental signal amongst noise; and determine if subtle variability in very young sediments can be identified at high-resolutions, guiding subsequent full-preparation and Single Aliquot Regenerative (SAR) (Murray and Wintle, 2000) dating methods on specific depths. Can subtle changes in chronostratigraphy be used to guide suitable sampling strategies in locations devoid of lithostratigraphic and micromorphological variation? This study

represents the first application of statistical changepoint analysis to luminescence datasets, and tests whether it is a viable tool to identify the depositional structure of visibly homogenous aeolian sediments using coarse L_x/T_x results. Near-surface aeolian dune sediments from the Nebraska Sandhills fulfilled the required criteria for this analysis. With the knowledge that these sediments have likely reactivated at a series of scales in the recent past, their visibly homogenous nature means that they are suitable sediments for the testing of this method.

2. Methods

2.1 Study site

The Nebraska Sandhills represent the largest dunefield in the Western Hemisphere (Loope and Swinehart, 2000; Ahlbrandt and Fryberger, 1980) and are currently stabilised by extensive prairie grassland. Existing research, as summarised in Halfen & Johnson (2013), has identified multiple Holocene reactivations using OSL dating throughout the Great Plains at 9.6-6.5ka, 3.8ka, 2.5ka (Miao et al., 2007), with the most recent regional-scale period spanning the Medieval Climatic Anomaly (MCA) 1050-650 years BP (Schmeisser McKean et al., 2014; Schmeisser et al., 2010; Forman et al., 2005; Goble et al., 2004; Mason et al., 2004; Loope and Swinehart, 2000; Stokes and Swinehart, 1997). Several less severe droughts have occurred after the MCA, such as during the 1930s Dust Bowl, that have caused increased areas of bare sand movement, but not complete reactivation as seen in the major droughts identified over the Holocene (Forman et al., 2005). Evidence from both the recent and more distant past has shown that aeolian activity has occurred repeatedly during the last 10,000 years at a variety of spatial scales.

2.2 Field sampling

A series of vertical sediment cores of approximately 50 cm depth were extracted from the upper surface sediments from dune and blowout features at two sites within the Nebraska Sandhills (Figure 2a): 1) The Gudmundsen Sandhills Laboratory (42.07575°N, 101.38680°W) and 2) – The Niobrara Valley Preserve and surrounding ranches (42.73719°N, 100.09194°W). Samples were extracted across transects which stretched across the topographic profile (i.e. from the crest / backwall of dunes, down the slopes and into the basin / interdune) of dune and blowout features with the aim of capturing sites of erosion and deposition within the local environment (Figure 2b & c). Vertical cores were extracted in situ by hammering 50 cm long light-tight tubes vertically into upper sedimentary sections, and transported to

the Oxford Luminescence Dating laboratory for analysis (Table 1). The quartz-rich dune sediments (Muhs, 2004) comprised of visually homogeneous aeolian material with a lack of stratigraphical boundaries and relatively consistent dose rates.

Sediment cores were opened and prepared under subdued orange light at the Oxford Luminescence Dating laboratory. Tubes were split lengthwise to allow subsampling of sediments at the centimetre scale, producing up to fifty sub-samples per core. Subsamples were left untreated and dried in the oven prior to luminescence measurement. One large aliquot (8mm diameter) per subsample was prepared on aluminium discs. Subsequent methods and measurements were applied to each subsampled unit unless otherwise stated.

2.3 Particle size variability

Particle size measurements were determined for a selection of sediment profiles, with subsample grain size data measured using a Malvern Mastersizer 3000 and analysed using GRADISTAT software version 8.0 (Blott and Pye, 2001). Sediment cores which appeared homogenous both visibly and in terms of particle size analysis were selected as appropriate test materials for this study.

2.4 L_x/T_x measurements on bulk samples

Measurements of L_x/T_x were made on individual aliquots, from samples spaced every 1 cm along each 50 cm core to provide a relative guide of luminescence variability with depth. Bulk signal OSL measurements were made using Risø TL/DA 15 readers, detecting using a 7.5mm Hoya U-340 filter. Single aliquot OSL blue luminescence measurements were conducted using 470 nm stimulation at 130°C for 100 s with a convex quartz lens placed in front of the photomultiplier tube for both the natural luminescence measurement (L_x) and the test dose measurement (T_x). A test dose of 6.5 Gy was used to standardise the natural bulk luminescence measurements along the depth of the individual sediment cores. Following a series of dose recovery and preheat plateau tests using fully-prepared samples (see Supplementary Information), a preheat of 200°C for 10 s was used prior to both the natural luminescence (L_x) and test dose luminescence (T_x) measurements at 130°C for 100 s.

2.5 Changepoint analysis

Whilst a qualitative visual assessment of structural breaks within the L_x/T_x depositional profile could be used to identify distinct points of change along a sediment core, an algorithmic approach is more suitable in this instance given the noisy nature of the dataset. All changepoint analysis was

completed using the Changepoint package (Killick and Eckley, 2014) in R Studio. The Changepoint analysis package identifies the location of breakpoints within the profile of each sediment core based on the variation in mean L_x/T_x measurements with depth. The pruned exact linear time (PELT) algorithm (Killick et al., 2012) was used, providing an exact segmentation unlike alternative methods (e.g. binary segmentation and segment neighbourhood algorithms) which represent a trade-off in speed and accuracy. Changepoint analysis requires the dataset to be in integer form; all L_x/T_x values were multiplied by 1,000 and rounded for this part of the analysis.

Within the changepoint analysis function, the user is required to enter a penalty value which determines the sensitivity of the model to changes within the dataset. Using a combination of the diagnostic plot and the argument that theoretically L_x/T_x should increase with depth, the model was repeated for each of the different penalty values identified in the CROPS (Changepoints for a Range of Penalties) option of the model. The final model per profile was selected as the output with the highest sensitivity to variability that continues to make stratigraphical sense. i.e. the number of changepoints within the dataset will increase until the model produces an output that suggests there are age reversals within the sedimentary core.

Identifying the optimum penalty value in this way ensures that both type 1 and type 2 errors (a type 1 error is the incorrect rejection of a true null hypothesis, while a type 2 error is incorrectly accepting a false null hypothesis) have been considered within the final model selection. Individual occasionally high and low L_x/T_x values that lie beyond the general range of the surrounding data points may have been influenced by a single K-feldspar or very sensitive quartz grain. Given the intrinsic variability expected within a prepared sample, as well as the aggregation of all grain sizes in this study, variability which is beyond intrinsic scatter, but is not indicative of a change in the depositional age, is expected. Consequently, the model is adjusted to not be too sensitive to individual changes and avoid each data point being identified as a distinctive break within the sequence. Equally, a very large penalty value that reduces the sensitivity of the model and fails to detect any changepoints within the series is not appropriate. A method to objectively identify the depositional structure of the sedimentary profile to subsequently allow focus on dating samples from a range of different age groupings is needed. Therefore, selecting the penalty value which produces a changepoint model which accommodates noise and variability anticipated within the dataset, whilst also making stratigraphical sense, is chosen to inform subsequent dating of the sediments (Figure 3).

2.6 SAR luminescence measurements

Based on the results from the changepoint analysis, mid-point subsamples from each of the identified changepoint sections were selected for full-preparation and SAR protocol (Wintle and Murray, 2006) luminescence measurement on prepared quartz. To test the validity of mid-point sub-samples in representing the general age of the wider changepoint sections, mid-point subsample ages were compared against a variety of fully-prepared SAR measurements from other subsamples within corresponding changepoint sections. Whilst multiple age estimates from the same changepoint section may increase the chronological resolution of the profile, they may not be required if the mid-point subsample proves to be representative of the identified section.

Samples were treated in an excess of HCl and H₂O₂ to remove carbonates and organics prior to wet-sieving to the appropriate size fraction (125-180 µm) and a 60 minute etch in 40% HF. A minimum of 16 small aliquots per sub-sample were measured following the SAR protocol (Wintle and Murray, 2006) with preheats (PH1 & PH2 – 200°C for 10s) determined following a series of preheat plateau and dose recovery tests. Single aliquot OSL blue luminescence measurements were conducted using 470 nm stimulation at 130°C for 100 s with a convex quartz lens placed in front of the photomultiplier tube. Recycling ratio tests and an IR-depletion ratio point were included to monitor sensitivity and identify any feldspar contamination (Duller, 2003). No significant recuperation was recorded along the length of the SAR cycle. Given the young nature of the sediments in this study, dose response curves were fitted against a linear function and individual equivalent dose estimates were calculated using interpolation of the natural signal onto this line. Uncertainties were calculated following 1,000 Monte Carlo fits of the line and propagated with a 2.5% measurement error. Sample equivalent doses were calculated using the unlogged Central Age Model (CAM) (Galbraith et al., 1999).

2.7 Dose rate calculation

Environmental dose rates were used to calculate age estimates for fully-prepared samples, and were determined by radionuclide (²³²Th, ²³⁸U and ⁴⁰K) concentrations measured using ICP-MS and calculated using the Dose Rate and Age Calculator (Durcan et al., 2015). Annual dose rates were calculated using standard conversion factors (Adamiec and Aitken, 1998) and adjusted for grain size (Mejdahl, 1979), HF-etching (Bell, 1979), beta attenuation and water content (Aitken, 1985). Cosmic dose rate was calculated following Prescott and Hutton (1994). Beta attenuation was corrected for using Guérin et al. (2011). Following the method described in Nelson and Rittenour (2015), soil moisture

content values were estimated using grain size characteristics, the van Genuchten (1980) water retention equation and Rosetta Lite v.1.1 software within the Hydrus-1D modelling program (Simunek et al., 2008). In situ moisture content values in semi-arid environments are unlikely to be representative of mean soil moisture conditions over the burial period of the sediment; so, an alternative modelling approach is used here.

2.8 Maximising signal potential

Given the young nature of the sediments being analysed, the luminescence measurements are characteristically dim with low OSL counts (typically < 200 counts in the first second). To maximise the signal size of these sediments a convex quartz lens was used to improve signal collection efficiency, and the impact of increasing photomultiplier tube (PMT) voltage was explored to improve the signal to noise ratio.

Using the same aliquots, a known dose was administered to the subsample and measured with and without the convex quartz lens at 130°C following a 10 s 200°C preheat (Figure 4). A convex quartz lens acts to focus the signal and therefore can increase the number of counts recorded in the photomultiplier tube. Measurements on eight samples showed that the inclusion of the convex quartz lens doubled the signal size of the aliquot (mean net signal ratio of 2.04) and reduced the size of the relative standard error associated with the luminescence signal by c.30%. Based on these results, the convex quartz lens was used in all luminescence measurements in this paper to improve signal-to-noise ratio and thus reduce uncertainties.

OSL counts over a 10 s integrated time window were measured five times and averaged with and without the calibration LED on at voltages between 600-1500 volts. The signal to noise ratio based on the average values suggests 1200 V as the optimum voltage for measurement conditions (Figure 5). Beyond 1200 V the signal-to-noise ratio decreases due to increased background OSL counts. 1200 V was used for all luminescence measurements made during this study.

3. Results

3.1 L_x/T_x profiles using bulk sample sediment

L_x/T_x data shown in Figure 6 demonstrate that L_x/T_x tends to increase with depth across all sediment cores analysed in this study. Further to this, the L_x/T_x profiles demonstrate the noisy nature of the bulk luminescence measurement dataset, and hence a method is needed to objectively identify changepoints within the record. As discussed earlier, the depositional structure of aeolian system profiles varies depending on the history of localised erosion and deposition that has occurred at that specific site. The results from this research demonstrate the high variability in the depositional structures that can be found between sediment cores taken from similar features within an individual site. Whilst all profiles show a general increase in L_x/T_x with depth, they equally show large amounts of inter-subsample variability which appear to increase as a function of increasing L_x/T_x – suggesting multiplicative errors.

3.2 Changepoint analysis on L_x/T_x profiles

L_x/T_x profiles from sediment cores taken across individual features have also been analysed to identify the utility of this method in detecting local relative variability in luminescence age across a feature (Figure 7). For example, there is clear variation in the L_x/T_x profiles across the sampling transect at site NVP16/4. Low and relatively homogenous values dominate the L_x/T_x profile at the crestal site (NVP16/4/1); little variability is detectable at this scale and across the 50 cm section. The slope sites (NVP16/4/2 and NVP16/4/4) both show similar L_x/T_x vs Depth profiles with L_x/T_x values < 0.2 dominating the shallower depths, whilst deeper sub-samples are characterised by higher L_x/T_x values and increased inter-aliquot variability. Finally, the basin of the dune profile (NVP16/4/3) shows the greatest range in L_x/T_x values across the length of the sediment core.

Figure 7 displays the results of changepoint analysis when applied to the four sedimentary cores taken across the NVP16/4 transect near Niobrara Valley Preserve. Coupling L_x/T_x profiles with changepoint analysis allows us to identify statistically significant shifts in the mean of the L_x/T_x measurements with depth.

The variability found between aliquots within a single changepoint section (Population B) was not statistically different to the variability identified between multiple measurements from the same depth (48 aliquots of 14 cm depth were measured – Population A) (Figure 8). This demonstrates that where 10-50 cm has been identified by the changepoint model as one distinct section, this section has the same variability as found between 48 discs at 14 cm depth. The variability found between repeat

measurements of the same depth is the same as that between depths down core that exhibit the same age.

Results of the original bulk measurements and changepoint output are compared against repeat L_x/T_x measurements across a selection of sediment cores in Figure 9. Whilst demonstrating an equally noisy response, the general trend and order of magnitude of the L_x/T_x measurements is the same between original and repeat measurements. Repeat measurements of the L_x/T_x vs Depth profiles show that similar results can be replicated despite the un-prepared nature of the sediments and the bulk signal measured. The output from the changepoint models show that there is some variability in the location of the break points identified between the original and repeat runs for the three cores tested, suggesting mid-point locations of the changepoint sections are more reproducible.

3.3 Age-depth profile estimates

Results testing whether mid-point age estimates using the SAR protocol are representative of the suggested changepoint sections are shown in Figure 10. Fully-prepared SAR ages for the mid-point subsample of each identified changepoint section were compared against age estimates produced for subsamples at every 5-10 cm for three sediment cores (Table 2). Mid-point subsamples were selected as the most appropriate subsamples to select for full-preparation dating as the location of the mid-point is reproducible in repeat measurements. Contrastingly, as noted in Figure 9 the exact location of the individual changepoints within the profile often varies between repeat runs due to noise, highlighting the risk in opting for an end-point to represent the wider section. Results show that luminescence ages from the same changepoint section are congruent (within errors); mid-point ages are broadly representative of the wider section. Likewise, fully prepared SAR ages are found to be indistinguishable to the mid-point age calculated, and different from the adjacent changepoint sections in sediment cores with multiple changepoints (Figure 10c). Individual dose rates have been calculated using ICP-MS radionuclide measurements for each SAR age estimate.

Overall, results showed that in these sediments, where no observable difference was found in sediment colour, sorting, or grain size (see Supplementary Information), L_x/T_x measurements and changepoint analysis were able to identify variation in sediment age. Sections that were visibly homogenous did not show any notable grain size variability. For example, results from the particle size analysis of sediment core NVP16/4/3 demonstrated a unimodal distribution of poorly-sorted medium-fine sands averaging 261 μm with a standard deviation 15 μm .

4. Discussion

4.1. Relative age profiles across a dune

Assuming L_x/T_x to be a proxy for age of deposition, the L_x/T_x profiles in Figure 7 allow us to identify relative changes in the ages of sediment across profiles of individual aeolian landforms. L_x/T_x can arguably be considered a good proxy for age in these young Nebraskan sediments where the dose rates show little variability, varying up to a maximum of c.0.25 Gy ka⁻¹ within each sediment core (Table 2), and the dose response is in the linear region (< 10 Gy) of the dose response curve; signal is proportional to age.

As expected, samples at the crestal site (Figure 7d) show low L_x/T_x readings throughout the 50 cm sedimentary core, suggesting modern age and a site of active sand movement. The two slope profiles (Figure 7e & g) demonstrate an increase in L_x/T_x with depth. No significant difference in particle size with depth, coupled with homogenous sands and no obvious horizon changes suggests that there is unlikely a large variation in the expected dose rate with depth and thus the L_x/T_x change can be assumed indicative of an increase in age. Given the untreated nature of the sediment, higher levels of variability between each aliquot than is normally identified in fully-prepared samples measuring isolated minerals and size fractions is expected. Finally, Figure 7 (f) shows a transition from young modern sand at the top of the core to much older sediments from c.36 cm onwards. If dose rates are homogenous, the oldest near-surface sediments across this profile are identified at the base of the dune, capped with modern sediments in the upper 17 cm. NVP16/4/3 is at present likely a source of sediment erosion, where a layer of bleached material overlies much older sediments which are gradually being deflated. In contrast, the slope profiles display an intermediary age sediment layer which does not appear to be represented within the basin (NVP16/4/3) profile. Uncertainty over depositional and erosional histories complicates the interpretation of the sediment cores. Deeper sediment cores taken from the slopes would confirm

whether the oldest material found in NVP16/4/3 is also preserved at deeper depths in the slope regions where less erosion and greater depositional activity has occurred.

The results demonstrate the utility of near-surface sediments as useful archives of environmental response to external disturbances. Near-surface sediments are under-represented in the published luminescence age record, due to concerns about the heterogeneity of the dose rate as well as bioturbation and reworking (Hesse, 2014). However, as Hesse (2014) notes, this theory relies on the assumption that the present is dissimilar to the past in that underlying sediments were not bioturbated when they once represented the surface layer. This study demonstrates that whilst variability is present, near-surface sediments can provide a useful insight into zones of reworking, erosion, and depositional structures across the profile of a landform. These core profiles are also useful in identifying the depth of surficial mixing and bleached material. In this example, the upper 50 cm at the crestal site appears to be modern, whilst this depth of “modern sand” changes across the dune transect. According to the slope profiles (Figure 7 e & g), the depth of modern sand ends at c.21 cm and 10 cm in cores NVP16/4/2 and NVP16/4/4 respectively.

Also of note is the change in level of centimetre-to-centimetre variability with increase in L_x/T_x (e.g. Figure 8 & 9). There are two potential reasons for this increased variability. Firstly, as sediments begin to accumulate a luminescence signal, inter-crystal and mineral variability will cause this signal to vary between sediments at a comparable level – this is expected and is encountered in all luminescence dating as the level of intrinsic variability. This level of variability is not noted in the modern sediments identified in the upper core and crestal sections where no significant (if any) luminescence dose has been stored. Proportionally, any dose that had accumulated in the young sediments would be significantly lower than the older deeper segments, and thus variability would expectedly be proportionally lower. Secondly, heterogeneity in the microdosimetry of the surrounding sediment will also cause variability between individual quartz grains, with this variability increasing in absolute terms with L_x/T_x .

4.2. Reproducing signals above noise

Reproducibility of the signal within a noisy dataset has been assessed at both the individual aliquot scale, and across depositional profiles. Figure 8 demonstrates that the L_x/T_x variability for a particular 1 cm-thick sample (population A), is the same as the variability found between subsamples within a deeper section (of tens of cm) defined as a single interval by changepoint analysis (population B). This suggests there is as much variability in L_x/T_x across a chronostratigraphic unit as there is within a

single sample at a single 1cm-thick depth. It was important to test this variability to be sure that the different changepoint model outcomes generated for the different sites in Figure 9 are real and not an artefact of variability in L_x/T_x for any one sample. i.e. is the inter-changepoint variability small enough to not impact the location of the breakpoints in the model.

Despite the variability in L_x/T_x for individual subsamples, the same broad sections are identified using the changepoint analysis algorithm (e.g. Figure 9b); highlighting that both type 1 and type 2 errors have adequately been accommodated for in the model selection criteria. Profiles which exhibited generally lower L_x/T_x values produced more variability between the original and repeat changepoint outputs, whilst increased congruency between repeats is found in profiles which exhibit higher L_x/T_x values (i.e. Figure 9b). The sedimentary cores which demonstrate lower L_x/T_x measurements show reduced levels of changepoint similarity between repeat runs. This is due to increased sensitivity in the model, which identifies changepoints which structurally are less significant. Contrastingly, a lower sensitivity model is required (higher penalty value) for the sediment cores which demonstrate distinct and true structural variability (i.e. NVP16/4/3 in Figure 9b). In this sense, the method is self-correcting whereby structural breakpoints which are significant and require a less sensitive model are more likely to be repeated in further repeat measurements of the same sediment profile. Meanwhile, breakpoints which are identified within a noisier setting with greater model sensitivity are structurally less significant.

The varying sensitivity requirement between models demonstrates the importance of identifying the appropriate penalty value to apply to the changepoint model for individual sedimentary sequences. In this study, the method is being used to identify changepoints within the profile where our dating efforts would be better focused, however subtle they might be, and subsequently inform further dating resources and interpretation. For example, the L_x/T_x profile in Figure 6 (m – GSL15/2/4) also shows a sedimentary sequence which has accumulated over time as a series of short and frequent pulsed depositional events as opposed to large and infrequent depositional events (e.g. Figure 6 (g – NVP16/4/3)). Yet the changepoint output for this profile identifies three sections within the profile, separated at 11 cm and 33 cm. It is important to recognise that all reactivation and deposition events are pulsed. The accumulation of sand grains cannot be truly continuous since they are distinct events occurring when the wind velocity required for sediment entrainment is reached and the sediment is available for transport. In this sense, despite appearing to sit on a straight line, there are always breaks in the sedimentary accumulation profile that perhaps could be described as quasi-continuous. Given the low L_x/T_x values and quasi-continuous nature of the profile, a lower penalty value was selected in this model to increase the sensitivity of the model to changes in the mean of the L_x/T_x values with depth (i.e. GSL15/2/4 penalty

value 6945, NVP16/4/3 penalty value 95979). The same penalty value (i.e. sensitivity) cannot be applied to all sedimentary profiles as the outputs would incorrectly identify age reversals in some of the sections, whilst missing subtle changes in the younger sections which have less distinct chronological breaks (Figure 11).

The likelihood that the changepoint model correctly identifies significant depositional breaks within the record is a function of its capacity to reproduce the same breakpoints with repeat measurements of the luminescence profile. Examples in this paper (e.g. Figure 9b) have shown that the self-correcting mechanism of the model sensitivity ensures that the most distinct structural changes are preserved between repeat measurements, whilst subtle variability attributed to noise will shift the breakpoints in sedimentary samples which have accumulated through short, frequent and quasi-continuous deposition events.

4.3. Predicting age-depth profiles from mid-point age estimates

Mid-point age estimates from changepoint sections have been found to be generally representative of the age bracket of the wider identified changepoint section. Nevertheless, the ability for the mid-point age to represent the whole section is ultimately determined by the sensitivity of the model and the age range covered within the sedimentary sequence. Age variation may occur within individually identified changepoint sections due to quasi-continuous accumulation of sediment within the same period of activation, and thus whilst the mid-point reflects the optimum location for measuring fully-prepared luminescence ages, additional ages will further improve the chronological resolution of the profile. For example, individual sections may demonstrate similar profiles to those found in Figure 6 (k) and (m), with gradually increasing L_x/T_x profiles punctuated by occasional step-changes in the depositional age – likely representing erosional boundaries or periods of pulsed deposition. Ultimately, the maximum information is achieved when the fully prepared luminescence ages are interpreted within the context of the depositional profile as identified in the L_x/T_x continuous measurements. These results demonstrate the utility of using changepoint analysis coupled with full-preparation dating techniques to produce a rapid age-depth profile of a sediment core, capturing the points of variability within the sedimentary profile whilst avoiding unnecessarily high volumes of sample dating. This positive result suggests that future sediment cores do not require a high-resolution chronology to reconstruct an age-depth profile that captures both accurate depositional ages and depositional structure within aeolian system sedimentary structures. The combination of L_x/T_x measurements, changepoint output and fully-prepared ages

produces rapid and accurate results that not only aids interpretation of individual sediment profiles, but also permits a greater spatial coverage of analysis which strengthens the overall reconstruction of environmental response within the landscape.

4.4. Complicating factors on sample age

One of the key assumptions of this study is that dose rate remains relatively homogeneous through each sediment core, suggesting the variability in L_x/T_x demonstrates changes in equivalent dose (i.e. age). This assumption is only valid in sediments which show homogenous sedimentary qualities and are not impacted by large volumes of heavy mineral contamination and are therefore subject to high levels of beta dose rate heterogeneity. Without any evidence for beta dose rate heterogeneity, dose rate changes over short spatial scales which generate high variability within the profile are not expected. However, in sedimentary environments which are quartz-dominated with very low levels of radionuclides, the soft component of the cosmic dose rate can be proportionally large and create a steep gradient of dose rate with depth in near-surface sediments. If dose rates are dominated by the cosmic dose rate component, caution should be taken when interpreting variability in L_x/T_x ; additional dates may be required to construct a more informed age-depth profile.

In this study, dose rates calculated using ICP-MS measurements have shown very little variability from top to bottom of the sediment cores (Table 2). For example, the means and standard deviations of the dose rate data calculated for sediment cores NVP15/1/1, NVP15/3/1 and NVP15/4/1 are $2.17 \pm 0.10 \text{ Gy ka}^{-1}$, $1.87 \pm 0.19 \text{ Gy ka}^{-1}$ and $2.62 \pm 0.16 \text{ Gy ka}^{-1}$ respectively. Coupled with relatively homogenous material, negligible grain size variability (e.g. mean and standard deviation of sediment core NVP16/3/2 grain size: $248 \pm 10 \mu\text{m}$ - see Supplementary Information for details), and a consistent sediment source over the time-period studied (and longer), there is little evidence to suggest that there would be strong variability in dose rates within the 50 cm core – except in locations where notably thick sod layers have been found overlying the dune sands. This conclusion is corroborated in the L_x/T_x profiles which consistently show an increase in L_x/T_x with depth. In addition, the high-resolution sampling in this study is comparable to making multiple measurements of the same sample under standard conditions, which would identify any significant levels of microscale dosimetry heterogeneity.

In sedimentary sections where variability in dose rate can be expected with depth (e.g. new field site, high volume of heavy minerals and zircons), each of the identified points for full-preparation dating should also be analysed for dose rate. The changepoint analysis allows us to crudely identify variability in the luminescence signal with depth which guides us for more thorough dating analysis. As part of this

analysis, each fully-prepared SAR measurement should be coupled with new dosimetry measurements to corroborate whether the changes in L_x/T_x have been induced by equivalent dose or dosimetry.

4.5. Application of this approach to longer time-series

Whilst this study has applied the changepoint technique to short sedimentary cores which are young in age (often < 200 years), this approach can equally be applied to deeper and older sedimentary sections. For longer sedimentary sequences a bi-sectioning method might be applied, progressively increasing the sampling and measuring of L_x/T_x of un-prepared bulk material until it shows no further stepped increases in values. For example, L_x/T_x measurements could be made at the top, middle and bottom of the core, and then additional measurements are made between the mid-points of the neighbouring points with the changepoint model re-run iteratively as each new L_x/T_x measurement is made. When the changepoint model no longer identifies any new changepoints (which conform to the model selection criteria), no further L_x/T_x measurements are required as the main breaks in the record have been identified. However, it should also be noted that for the same difference in age with older sediments, the difference in L_x/T_x values will be subtler when the ages of samples are above the linear section of the dose response curve. As age increases, the L_x/T_x values will appear closer until saturation of the dose response curve is reached and they will no longer produce any variation in L_x/T_x values. It is therefore expected that this method will become less sensitive as age increases, and this remains to be explored in future applications. A combination which incorporates portable luminescence reader measurements is likely more appropriate on significantly longer sedimentary sections to help guide sample strategy.

Each fully-prepared SAR age should be coupled with a new assessment of the dose rate at that corresponding depth to confirm if the notable changes in L_x/T_x occurred as a factor of age or dose rate. Increasing the number of L_x/T_x measurements in the changepoint model will improve the accuracy in identifying the breakpoints in the depositional profile. However, as noted this would rely on the assumption that the dose rate and sensitivity of the sediments has not changed significantly through the sedimentary core. Notable stratigraphic layers and structures within the sample core should also be used to guide the sub-sampling and L_x/T_x measurements.

5. Conclusions

This study has presented a new method for identifying chronological change in visibly homogenous dune depositional profiles. Using an algorithmic approach, this study represents the first application of changepoint analysis to a luminescence dataset and has demonstrated the utility of such methods in focusing dating efforts when investigating aeolian system dynamics. High-volume sampling of visibly homogenous sediments can successfully capture chronostratigraphic variability when combined with statistical changepoint analysis to identify the breakpoints in the chronostratigraphy. Despite the unprepared nature of the sediment samples, this research has demonstrated the possibility of measuring subtle changes in luminescence with depth, allowing us to identify step-changes in the depositional age of near-surface sediments. The significant reduction in preparation time is successful in allowing for rapid relative age assessment prior to in-depth accurate age generation using luminescence techniques. Whilst the sediments used in this example were young in depositional age (i.e. decades to century-scale) with expectedly weak luminescence signals, the large aliquots coupled with the convex quartz lens and the higher voltage used in the measuring of the signal allowed for optimisation of the signal size. Naturally occurring high dose rates (c.2.2 Gy/ka) in the region also provide suitable sediments for attempting to measure at the very young end of the age spectrum.

When considered together across an individual geomorphological feature within the aeolian system, multiple L_x/T_x profiles provide a relative age assessment that can help inform our understanding of the processes of erosion and deposition across individual features. Coupled with changepoint analysis and model selection criteria, the results have shown the potential to identify step-changes within L_x/T_x profiles which can focus dating efforts on points of change within the depositional setting. Further to this, in sedimentary sections devoid of significant lithological and mineralogical change, single fully-prepared SAR luminescence ages taken at the mid-point of identified changepoint sections can be used to produce age-depth profiles of near-surface sediments, reducing the need to date all sediment samples. Importantly, this study has confirmed the pulsed depositional nature of aeolian system sedimentary profiles and demonstrated a method which allows researchers to interpret luminescence ages within the context of a depositional structure. A method which combines depositional structure with chronology is particularly important in contributing to our overall understanding of what a luminescence date represents within the context of an individual sample or geomorphological feature. The findings presented demonstrate that L_x/T_x measurements coupled with changepoint analysis modelling of near-surface sediment cores provide a suitable method for reconstructing an environmental signal in an aeolian

system characterised by high-volumes of environmental noise. What's more, this relatively quick approach, combining coarse L_x/T_x measurements with the use of the changepoint algorithm, facilitates a better informed full-preparation dating approach where excess samples are not dated in order to produce accurate age-depth profiles.

Acknowledgements

This work was supported by the UK Natural Environmental Research Council (grant: NE/L002612/1), Jesus College Graduate Research Allowance funding, and Elsevier Travel Grant (October 2015). The first author is funded by NERC (grant: NE/L002612/1) as part of the Environmental Research Doctoral Training Program at the University of Oxford. We thank Drs Paul Hanson and Dave Wedin (University of Nebraska-Lincoln), The Nature Conservancy and the staff at Niobrara Valley Preserve, Al and Lois Steuter and Larry O'Keif, and the staff at Gudmundsen Sandhills Laboratory for support, assistance and field site access. The authors would like to thank the anonymous reviewers for their comments on an earlier draft of the manuscript.

References

- Adamiec G. and Aitken M., 1998. Dose-rate conversion factor: update. *Anc. TL*.
- Ahlbrandt, T.S., Fryberger, S.G., 1980. Eolian deposits in the Nebraska Sand Hills, *Geologic and Paleocologic Studies of the Nebraska Sand Hills*.
- Aitken, M., 1985. *Thermoluminescence Dating*. London, Academic Press Inc.
- Atkinson, O.A.C., Thomas, D.S.G., Goudie, A.S., Bailey, R.M., 2011. Late Quaternary chronology of major dune ridge development in the northeast Rub' al-Khali, United Arab Emirates. *Quat. Res.* 76, 93–105. <https://doi.org/10.1016/j.yqres.2011.04.003>
- Bailey, R.M., Thomas, D.S.G., 2014. A quantitative approach to understanding dated dune stratigraphies. *Earth Surf. Process. Landforms* 39, 614–631. <https://doi.org/10.1002/esp.3471>
- Bateman, M.D., Rushby, G., Stein, S., Ashurst, R.A., Stevenson, D., Jones, J.M., Gehrels, W.R., 2017. Can sand dunes be used to study historic storm events? *Earth Surf. Process. Landforms* 2. <https://doi.org/10.1002/esp.4255>
- Bateman, M.D., Stein, S., Ashurst, R.A., Selby, K., 2015. Instant luminescence chronologies? High

- 678 resolution luminescence profiles using a portable luminescence reader. *Quat. Geochronol.* 30, 141–
679 146. <https://doi.org/10.1016/j.quageo.2014.12.007>
- 680 Bell, W.T., 1979. Thermoluminescence Dating: Radiation dose-rate data. *Archaeometry* 21, 243–245.
- 681 Blott, S.J., Pye, K., 2001. Gradistat: A Grain Size Distribution and Statistics Package for the Analysis of
682 Unconsolidated Sediments. *Earth Surf. Process. Landforms* 26, 1237–1248.
683 <https://doi.org/10.1002/esp.261>
- 684 Chase, B., 2009. Evaluating the use of dune sediments as a proxy for palaeo-aridity: A southern African
685 case study. *Earth-Science Rev.* 93, 31–45. <https://doi.org/10.1016/j.earscirev.2008.12.004>
- 686 Duller, G.A.T., 2003. Distinguishing quartz and feldspar in single grain luminescence measurements.
687 *Radiat. Meas.* 37, 161–165. [https://doi.org/10.1016/S1350-4487\(02\)00170-1](https://doi.org/10.1016/S1350-4487(02)00170-1)
- 688 Durcan, J.A., King, G.E., Duller, G.A.T., 2015. DRAC: Dose Rate and Age Calculator for trapped charge
689 dating. *Quat. Geochronol.* 28, 54–61. <https://doi.org/10.1016/j.quageo.2015.03.012>
- 690 Durcan, J.A., Roberts, H.M., Duller, G.A.T., Alizai, A.H., 2010. Testing the use of range-finder OSL dating
691 to inform field sampling and laboratory processing strategies. *Quat. Geochronol.* 5, 86–90.
692 <https://doi.org/10.1016/j.quageo.2009.02.014>
- 693 Fitzsimmons, K.E., Rhodes, E.J., Magee, J.W., Barrows, T.T., 2007. The timing of linear dune activity in
694 the Strzelecki and Tirari Deserts, Australia. *Quat. Sci. Rev.* 26, 2598–2616.
695 <https://doi.org/10.1016/j.quascirev.2007.06.010>
- 696 Fitzsimmons, K.E., Telfer, M.W., 2008. Sedimentary History and the Interpretation of Late Quaternary
697 Dune Records: Examples from the Tirari Desert, Australia and the Kalahari, South Africa.
698 *ChungaraRevista Antropol. Chil.* 40, 295–308 ST–Sedimentary History and the Interpre.
699 <https://doi.org/10.4067/S0717-73562008000300006>
- 700 Forman, S.L., Marín, L., Pierson, J., Gómez, J., Miller, G.H., Webb, R.S., 2005. Aeolian sand
701 depositional records from western Nebraska: landscape response to droughts in the past 1500
702 years. *The Holocene* 15, 973–981. <https://doi.org/10.1191/0959683605hl871ra>
- 703 Fryberger, S.G., 1979. Dune forms and wind regime, in: McKee, E.D. (Ed.), *A Study of Global Sand Seas*
704 (US Geological Survey Professional Paper 1052). Reston, VA: US Geological Survey, pp. 137–
705 169.
- 706 Galbraith, R.F., Roberts, R.G., Laslett, G.M., Yoshida, H., Olley, J.M., 1999. Optical dating of single and
707 multiple grains of quartz from jinnium rock sheltern, northern Australia: Part I, experimental design
708 and statistical models. *Archaeometry* 41, 339–364. [https://doi.org/10.1111/j.1475-](https://doi.org/10.1111/j.1475-4754.1999.tb00987.x)
709 [4754.1999.tb00987.x](https://doi.org/10.1111/j.1475-4754.1999.tb00987.x)

- Goble, R.J., Mason, J. a., Loope, D.B., Swinehart, J.B., 2004. Optical and radiocarbon ages of stacked paleosols and dune sands in the Nebraska Sand Hills, USA. *Quat. Sci. Rev.* 23, 1173–1182. <https://doi.org/10.1016/j.quascirev.2003.09.009>
- Guérin, G., Mercier, N., Adamiec, G., 2011. Dose-rate conversion factors : update 29, 5–8.
- Halfen, A.F., Johnson, W.C., 2013. A review of Great Plains dune field chronologies. *Aeolian Res.* 10, 135–160. <https://doi.org/10.1016/j.aeolia.2013.03.001>
- Hesse, P.P., 2014. How do longitudinal dunes respond to climate forcing? Insights from 25 years of luminescence dating of the Australian desert dunefields. *Quat. Int.* 1–19. <https://doi.org/10.1016/j.quaint.2014.02.020>
- Hughes, P.D., 2010. Geomorphology and Quaternary stratigraphy: The roles of morpho-, litho-, and allostratigraphy. *Geomorphology* 123, 189–199. <https://doi.org/10.1016/j.geomorph.2010.07.025>
- Killick, R., Eckley, I., 2014. changepoint: An R Package for changepoint analysis. *Lancaster Univ.* 58, 1–15. <https://doi.org/10.1359/JBMR.0301229>
- Killick, R., Fearnhead, P., Eckley, I. a., 2012. Optimal detection of changepoints with a linear computational cost. *J. Am. Stat. Assoc.* 107, 1590–1598. <https://doi.org/10.1080/01621459.2012.737745>
- Kocurek, G., Lancaster, N., 1999. Aeolian system sediment state: Theory and Mojave Desert Kelso dune field example. *Sedimentology* 46, 505–515. <https://doi.org/10.1046/j.1365-3091.1999.00227.x>
- Leighton, C.L., Bailey, R.M., 2015. Investigating the potential of HCl-only treated samples using range-finder OSL dating. *Quat. Geochronol.* 25, 1–9. <https://doi.org/10.1016/j.quageo.2014.08.002>
- Leighton, C.L., Thomas, D.S.G., Bailey, R.M., 2014. Reproducibility and utility of dune luminescence chronologies. *Earth-Science Rev.* 129, 24–39. <https://doi.org/10.1016/j.earscirev.2013.11.007>
- Leighton, C.L., Thomas, D.S.G., Bailey, R.M., 2013. Allostratigraphy and Quaternary dune sediments: Not all bounding surfaces are the same. *Aeolian Res.* 11, 55–60. <https://doi.org/10.1016/j.aeolia.2013.09.001>
- Lomax, J., Hilgers, A., Radtke, U., 2011. Palaeoenvironmental change recorded in the palaeodunefields of the western Murray Basin, South Australia - New data from single grain OSL-dating. *Quat. Sci. Rev.* 30, 723–736. <https://doi.org/10.1016/j.quascirev.2010.12.015>
- Loope, D.B., Swinehart, J.B., 2000. Thinking Like a Dune Field: Geologic History in the Nebraska Sand Hills. *Gt. Plains Res.* 10, 5–35.
- Mason, J. a., Swinehart, J.B., Goble, R.J., Loope, D.B., 2004. Late-Holocene dune activity linked to hydrological drought, Nebraska Sand Hills, USA. *The Holocene* 14, 209–217.

<https://doi.org/10.1191/0959683604hl677rp>

- Mejdahl, V., 1979. Thermoluminescence Dating: Beta-dose attenuation in quartz grains. *Archaeometry* 21, 61–72.
- Miao, X., Mason, J. a., Swinehart, J.B., Loope, D.B., Hanson, P.R., Goble, R.J., Liu, X., 2007. A 10,000 year record of dune activity, dust storms, and severe drought in the central Great Plains. *Geology* 35, 119–122. <https://doi.org/10.1130/G23133A.1>
- Muhs, D.R., 2004. Mineralogical maturity in dunefields of North America, Africa and Australia. *Geomorphology* 59, 247–269. <https://doi.org/10.1016/j.geomorph.2003.07.020>
- Munyikwa, K., 2005. The role of dune morphogenetic history in the interpretation of linear dune luminescence chronologies: a review of linear dune dynamics. *Prog. Phys. Geogr.* 29, 317–336. <https://doi.org/10.1191/0309133305pp451ra>
- Murray, A.S., Wintle, A.G., 2000. Luminescence dating of quartz using an improved single-aliquot regenerative-dose protocol. *Radiat. Meas.* 32, 57–73. [https://doi.org/10.1016/S1350-4487\(99\)00253-X](https://doi.org/10.1016/S1350-4487(99)00253-X)
- Nelson, M.S., Rittenour, T.M., 2015. Using grain-size characteristics to model soil water content: Application to dose-rate calculation for luminescence dating. *Radiat. Meas.* 81, 142–149. <https://doi.org/10.1016/j.radmeas.2015.02.016>
- Prescott, J.R., Hutton, J.T., 1994. Cosmic ray contributions to dose rates for luminescence and ESR dating: Large depths and long-term time variations. *Radiat. Meas.* 23, 497–500. [https://doi.org/10.1016/1350-4487\(94\)90086-8](https://doi.org/10.1016/1350-4487(94)90086-8)
- Roberts, H.M., Durcan, J.A., Duller, G.A.T., 2009. Exploring procedures for the rapid assessment of optically stimulated luminescence range-finder ages. *Radiat. Meas.* 44, 582–587. <https://doi.org/10.1016/j.radmeas.2009.02.006>
- Sanderson, D.C.W., Murphy, S., 2010. Quaternary Geochronology Using simple portable OSL measurements and laboratory characterisation to help understand complex and heterogeneous sediment sequences for luminescence dating. *Quat. Geochronol.* 5, 299–305. <https://doi.org/10.1016/j.quageo.2009.02.001>
- Schmeisser, R.L., Loope, D.B., Mason, J. a., 2010. Modern and late Holocene wind regimes over the Great Plains (central U.S.A.). *Quat. Sci. Rev.* 29, 554–566. <https://doi.org/10.1016/j.quascirev.2009.11.003>
- Schmeisser McKean, R.L., Goble, R.J., Mason, J.B., Swinehart, J.B., Loope, D.B., 2014. Temporal and spatial variability in dune reactivation across the Nebraska Sand Hills, USA. *The Holocene* 25, 523–

535. <https://doi.org/10.1177/0959683614561889>
- Simunek, J., Senja, M., van Genuchten, M.T., 2008. Code for simulating the one-dimensional movement of water, heat, and multiple solutes in variably saturated porous media: Hydrus-1D, Version 4.16.0090. USDA-ARS, California.
- Singhvi, A.K., Porat, N., 2008. Impact of luminescence dating on geomorphological and palaeoclimate research in drylands. *Boreas* 37, 536–558. <https://doi.org/10.1111/j.1502-3885.2008.00058.x>
- Stevens, T., Armitage, S.J., Lu, H., Thomas, D.S.G., 2006. Sedimentation and diagenesis of Chinese loess: Implications for the preservation of continuous, high-resolution climate records. *Geology* 34, 849–852. <https://doi.org/10.1130/G22472.1>
- Stokes, S., Swinehart, J.B., 1997. Middle- and late-Holocene dune reactivation in the Nebraska Sand Hills, USA. *The Holocene* 7, 263–272.
- Stone, A.E.C., Bateman, M.D., Thomas, D.S.G., 2015. Rapid age assessment in the Namib Sand Sea using a portable luminescence reader. *Quat. Geochronol.* 30, 134–140. <https://doi.org/10.1016/j.quageo.2015.02.002>
- Stone, A.E.C., Thomas, D.S.G., 2008. Linear dune accumulation chronologies from the southwest Kalahari, Namibia: challenges of reconstructing late Quaternary palaeoenvironments from aeolian landforms. *Quat. Sci. Rev.* 27, 1667–1681. <https://doi.org/10.1016/j.quascirev.2008.06.008>
- Telfer, M.W., Bailey, R.M., Burrough, S.L., Stone, A.E.S., Thomas, D.S.G., Wiggs, G.S.F., 2010. Understanding linear dune chronologies: Insights from a simple accumulation model. *Geomorphology* 120, 195–208. <https://doi.org/10.1016/j.geomorph.2010.03.030>
- Telfer, M.W., Hesse, P.P., Perez-Fernandez, M., Bailey, R.M., Bajkan, S., Lancaster, N., 2017. Morphodynamics, boundary conditions and pattern evolution within a vegetated linear dunefield. *Geomorphology* 290, 85–100. <https://doi.org/10.1016/j.geomorph.2017.03.024>
- Telfer, M.W., Thomas, D.S.G., 2007. Late Quaternary linear dune accumulation and chronostratigraphy of the southwestern Kalahari: implications for aeolian palaeoclimatic reconstructions and predictions of future dynamics. *Quat. Sci. Rev.* 26, 2617–2630. <https://doi.org/10.1016/j.quascirev.2007.07.006>
- Thomas, D.S.G., 2013. Reconstructing paleoenvironments and palaeoclimates in drylands: what can landform analysis contribute? *Earth Surf. Process. Landforms* 38, 3–16. <https://doi.org/10.1002/esp.3190>
- Thomas, D.S.G., Bailey, R.M., 2017. Is there evidence for global-scale forcing of southern hemisphere Quaternary desert dune accumulation? A quantitative method for testing hypotheses of dune system development. *Earth Surf. Process. Landforms.* <https://doi.org/10.1002/esp.4183>

- 806 Thomas, D.S.G., Burrough, S.L., 2013. Luminescence-based dune chronologies in southern Africa:
807 Analysis and interpretation of dune database records across the subcontinent. *Quat. Int.*
808 <https://doi.org/10.1016/j.quaint.2013.09.008>
- 809 Thomas, D.S.G., Burrough, S.L., 2012. Interpreting geoproxies of late Quaternary climate change in
810 African drylands: Implications for understanding environmental change and early human behaviour.
811 *Quat. Int.* 253, 5–17. <https://doi.org/10.1016/j.quaint.2010.11.001>
- 812 van Genuchten, M.T., 1980. A closed-form equation for predicting the hydraulic conductivity of
813 unsaturated soils. *Soil Sci. Soc. Am. J.* 44, 892–898.
- 814 Wintle, A.G., Murray, A.S., 2006. A review of quartz optically stimulated luminescence characteristics and
815 their relevance in single-aliquot regeneration dating protocols. *Radiat. Meas.* 41, 369–391.
816 <https://doi.org/10.1016/j.radmeas.2005.11.001>
- 817 Wolfe, S.A., Nickling, W.G., 1993. The protective role of sparse vegetation in wind erosion. *Prog. Phys.*
818 *Geogr.* 17, 50–68. <https://doi.org/10.1177/030913339301700104>
- 819

Figure 1. A representation of the assumptions made about depositional structure when sedimentary sections are under-sampled. (a) Sedimentary profile that has accumulated gradually over time in a quasi-continuous manner. (b) Sedimentary profile that has accumulated in pulsed events over time. Sampling at only two locations and inferring a linear relationship can mask the true structure and complexity of the underlying profile.

Figure 2. (a) Location map of the Niobrara Valley Preserve and Gudmundsen Sandhills Laboratory within the Nebraska Sandhills. (b) Map of the Gudmundsen Sandhills Laboratory showing sites where vertical sediment cores were extracted. 41 sediment cores extracted across the sites (A-J). A: GSL15/1/1, B: GSL15/2 (8 cores), C: GSL16/1 (4 cores), D: GSL16/2 (4 cores), E: GSL16/3 (4 cores), F: GSL16/4 (4 cores), G: GSL16/5 (4 cores), H: GSL16/6 (4 cores), I: GSL16/7 (4 cores), J: GSL16/8 (4 cores). (c) Map of Niobrara Valley Preserve and surrounding ranches showing sites where vertical sediment cores were extracted. 25 sediment cores were extracted across the sites (A-H). A: NVP15/1/1 & NVP15/3/1, B: NVP15/4/1, C: NVP16/1 (4 cores), D: NVP16/2 (4 cores), E: NVP16/3 (4 cores), F: NVP16/4 (4 cores), G: NVP16/5 (4 cores), H: NVP16/6 (2 cores). See Figure 7a for an example of sampling transects and 7b for image of visually homogenous sediment during core extraction.

Table 1. Sediment cores specifically referred to in this paper. Table details geomorphic setting, depth, latitude, longitude and elevation of the extracted cores. Site reference on Figure 2 is denoted in brackets for each vertical sediment core.

Figure 3. (a-d) Changepoint model outputs for sediment core NVP16/4/3 based on different levels of model sensitivity. (a) is an example where penalty value was set high and no changepoints were detected in the data sequence. Whereas in (d) the penalty value is very low and the model is overly sensitive to every change within the dataset. Based on the law of superposition, the sediments are expected to get older with depth and therefore reject the overly sensitive models which assume age reversals. Model output (c) has been selected as the most appropriate output for this example.

Figure 4. (a) OSL depletion curve of NVP15/4/1/21 with and without a convex quartz lens placed in front of the photomultiplier tube. (b) Ratio of 'with quartz convex quartz lens' to 'without convex quartz lens' signal size per channel of measurement.

Figure 5. a) Calibration LED OSL counts / Background OSL counts vs. Voltage. Ratio plateaus from 1100-1200 V onwards. b) Background OSL counts vs. Voltage. Background OSL counts increase as a function of voltage.

Figure 6. (a-j) L_x/T_x vs. Depth (cm below surface) profiles of un-prepared sediment samples from ten cores taken at the Niobrara Valley Preserve site. (k-t) L_x/T_x vs. Depth (cm below surface) profiles of un-prepared sediment samples from ten cores taken at the Gudmundsen Sandhills Laboratory site. All sub-figures show noisy L_x/T_x datasets which consistently increase with depth. Fig 6 (e), (k), (l), (m) and (q) show examples of profiles with L_x/T_x values gradually increasing, suggesting these

sediments have accumulated linearly over the period covered in the sediment core. Contrastingly, (n) & (t) appear to show more distinct populations of sediments which might suggest a depositional profile which has accumulated through pulsed depositional events, or which has been post-depositionally eroded over time. (c), (g) & (p) are good examples of the range of ages that have been found within the shallow 50 cm cores, showing distinct populations of sediment which get older with depth. See Table 1 for GPS co-ordinates for individual cores.

Figure 7. (a) Transect NVP16/4 and the location of the four sediment cores extracted (Site F on Figure 2 Niobrara Valley Preserve map). Satellite imagery courtesy of © 2017 Google Earth Pro, Landsat / Copernicus. (b) Example of vertical sediment core in situ. (c) Side profile of transect NVP16/4 across blowout feature formed against the fence line of a historic homestead site near to the Niobrara Valley Preserve. (d-g) L_x/T_x vs. Depth profiles for sediment cores NVP16/4/1, NVP16/4/2, NVP16/4/3 and NVP16/4/4 (crest, slope, basin, slope) across transect with changepoint outputs. Changepoints identified as breaks in the horizontal red lines. (d) Changepoint output plot for sediment core NVP16/4/1 identified two distinct changes in the means of the samples at 8 and 44 cm. (e) Changepoint output plot for sediment core NVP16/4/2 one distinct change in the means of the samples at 25 cm. (f) Changepoint output plot for sediment core NVP16/4/3 identified two distinct changes in the means of the samples at 21 cm and 37 cm. (g) Changepoint output plot for sediment core NVP16/4/4 taken from the slope of the blowout feature identified one distinct change in the means of the samples at 10 cm. L_x/T_x values were multiplied by 1000 for changepoint analysis.

Figure 8. Plot showing L_x/T_x vs. Depth for sediment core NVP16/4/4. Changepoint analysis identified two distinct sections within the profile split at 10 cm depth. Population A shows the repeat L_x/T_x measurements for 48 aliquots of NVP16/4/4/14. Population B shows the distribution of L_x/T_x measurements for the aliquots measured from 13-49cm down core. ANOVA single factor analysis shows that there is no significant difference between Populations A and B.

Figure 9. Original (crosses) and repeat runs (filled circles) of L_x/T_x vs. Depth profiles coupled with Changepoint analysis of each run. (a) Original and repeat analysis of sediment core NVP15/4/1 – changepoints identified at 17 and 43 cm in original analysis and 7 and 22 cm in repeat measurements. (b) Original and repeat analysis of sediment core NVP16/4/3 – changepoints identified at 21 and 37 cm in original analysis and 19, 34 and 42 cm in repeat measurements. (c) Original and repeat analysis of sediment core NVP16/5/1 – changepoints identified at 12, 23 and 38 cm in original analysis and 19 and 32 cm in repeat measurements. Breaks in the red lines represent changepoints in the sample means identified.

Figure 10. (upper) L_x/T_x profiles for sediment cores (a) NVP15/1/1, (b) NVP15/3/1, and (c) NVP15/4/1 coupled with changepoint model outputs. (lower) Fully-prepared SAR age estimates – sample in red denotes mid-point subsample from identified changepoint section. Grey dashed lines demarcate populations of ages that demonstrate similar results. Fully-prepared SAR OSL age estimates listed in Table 3.

Table 2. OSL results for sediment cores NVP15/1/1, NVP15/3/1 and NVP15/4/1. All sub-sample ages were calculated using overburden density $1.9 \pm 0.1 \text{ g/cm}^3$ and water content value of $3 \pm 2 \%$ following the method described in Nelson and Rittenour (2015). n is number of aliquots measured.

^a Depth of sub-sample below modern land surface

^b Equivalent dose (Gy)

^c U (ppm), Th (ppm) and K (%) calculated based on individual radionuclide measurements

^d Cosmic ray dose rate calculated based on sample elevation, latitude, longitude and depth of burial (Prescott and Hutton, 1994)

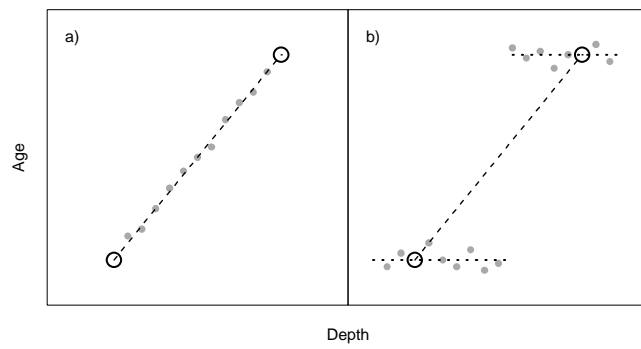
^e Total dose rate calculated using DRAC (Durcan et al., 2015)

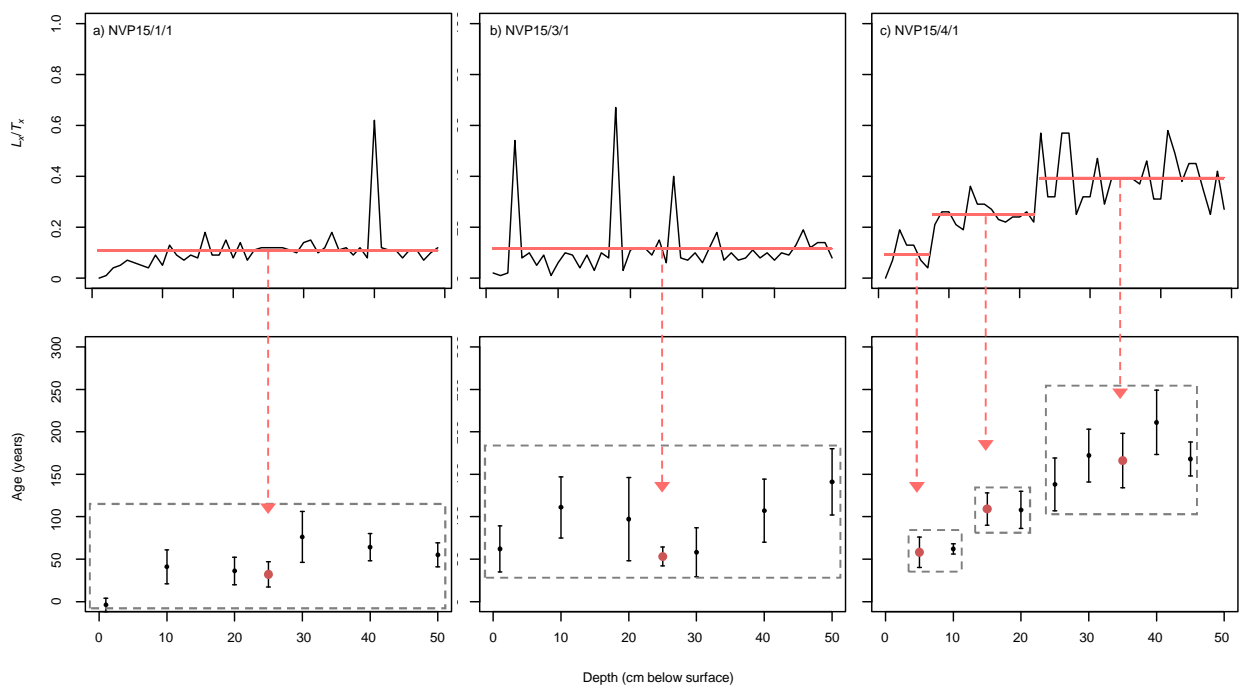
^f Years before 2015 AD

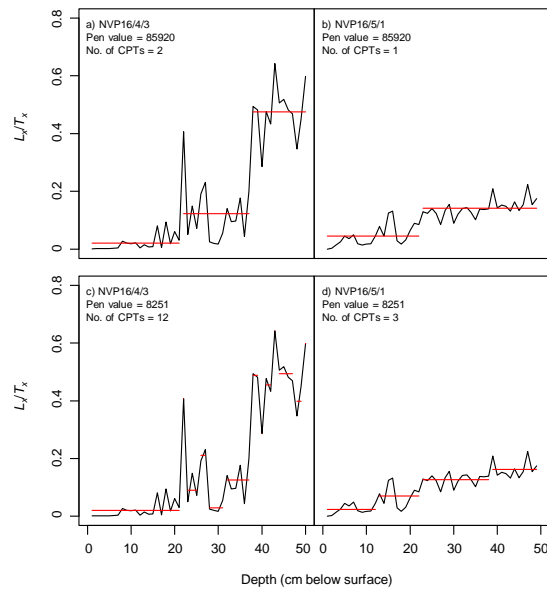
Figure 11. Changepoint model outputs for two sediment cores when different levels of model sensitivity are applied. Relatively low model sensitivity has been applied to outputs (a) and (b) for sediment cores NVP16/4/3 and NVP16/5/1 respectively. Relatively high model sensitivity has been applied to outputs (c) and (d) for NVP16/4/3 and NVP16/5/1 respectively. With reduced sensitivity, fewer changepoints are identified in NVP16/5/1, yet higher model sensitivity identifies additional changepoints within NVP16/4/3 which theoretically do not make sense as they suggest age-reversals.

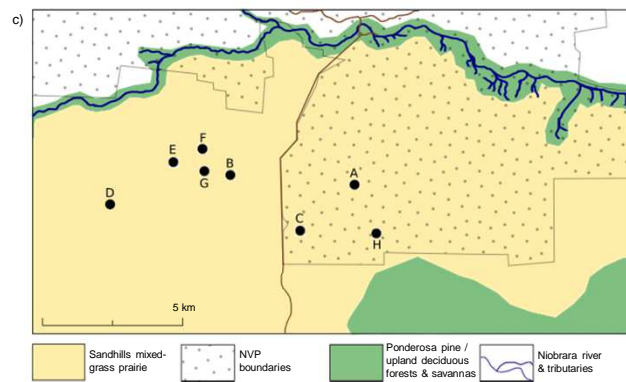
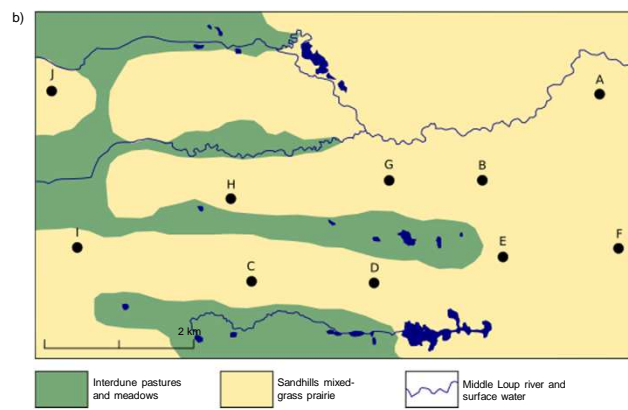
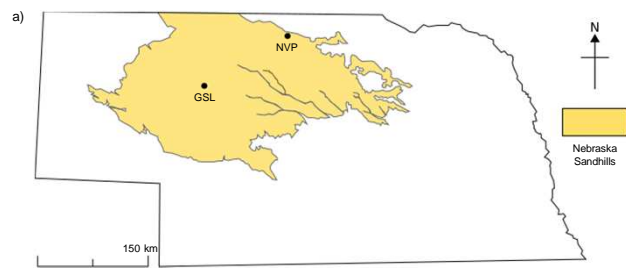
Core	Geom. setting	Depth (m)	Latitude	Longitude	Elevation (m a.s.l.)
NVP15/1/1 (A)	Crest	0 - 0.5	42.73510°	-100.03734°	768
NVP15/3/1 (A)	Basin	0 - 0.5	42.73491°	-100.03781°	757
NVP15/4/1 (B)	Crest	0 - 0.5	42.73719°	-100.09194°	761
NVP16/2/2 (D)	Lower ridge	0 - 0.5	42.72723°	-100.14481°	782
NVP16/2/3 (D)	Slope	0 - 0.5	42.72713°	-100.14458°	781
NVP16/4/1 (F)	Crest	0 - 0.5	42.74444°	-100.10461°	768
NVP16/4/2 (F)	Slope	0 - 0.5	42.74437°	-100.10448°	764
NVP16/4/3 (F)	Basin	0 - 0.5	42.74415°	-100.10422°	759
NVP16/4/4 (F)	Slope	0 - 0.5	42.74380°	-100.10403°	751
NVP16/5/1 (G)	Crest	0 - 0.5	42.71943°	-100.02847°	763
NVP16/5/2 (G)	Slope	0 - 0.5	42.71943°	-100.02880°	762
GSL15/1/1 (A)	Blowout back wall	0 - 0.5	42.08627°	-101.36721°	1078
GSL16/1/3 (C)	Depression	0 - 0.5	42.06317°	-101.42488°	1113
GSL15/2/4 (B)	Crest	0 - 0.5	42.07575°	-101.38680°	1109
GSL16/2/4 (D)	Slope	0 - 0.5	42.06240°	-101.40483°	1079
GSL16/3/2 (E)	Depression	0 - 0.5	42.06588°	-101.38376°	1074
GSL16/4/3 (F)	Depression	0 - 0.5	42.06719°	-101.36451°	1066
GSL16/5/1 (G)	Crest	0 - 0.5	42.0755°	-101.40309°	1099
GSL16/5/3 (G)	Depression	0 - 0.5	42.07536°	-101.40255°	1093
GSL16/5/4 (G)	Gully	0 - 0.5	42.07515°	-101.40218°	1085
GSL16/7/1 (I)	Crest	0 - 0.5	42.06775°	-101.45338°	1140

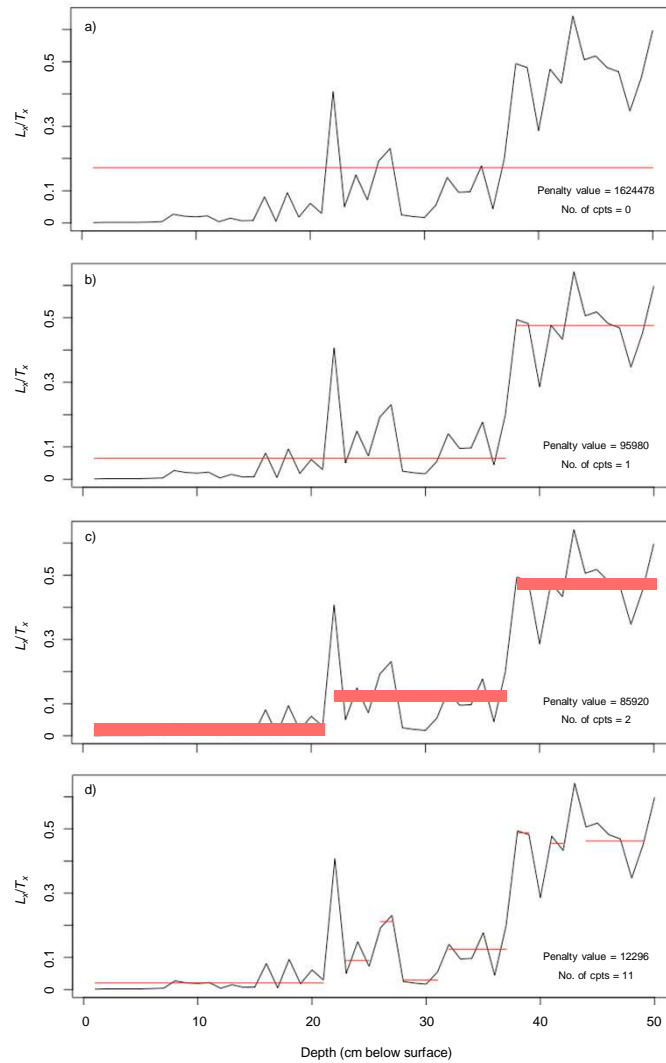
Sample	Depth (cm) ^a	<i>n</i>	<i>D_e</i> (Gy) ^b	Grainsize (μ m)	K (%) ^c	Th (ppm) ^c	U (ppm) ^c	<i>D_{cosmic}</i> (Gy ka ⁻¹) ^d	<i>D_{total}</i> (Gy ka ⁻¹) ^e	Age (years) ^f
NVP15/1/1/1	1	25	-0.0069 \pm 0.02	125-180	1.54 \pm 0.031	3.6 \pm 0.072	0.8 \pm 0.016	0.33 \pm 0.03	1.97 \pm 0.12	-4 \pm 8
NVP15/1/1/10	10	19	0.087 \pm 0.042	125-180	1.54 \pm 0.031	3.6 \pm 0.072	0.8 \pm 0.016	0.30 \pm 0.03	2.12 \pm 0.13	41 \pm 20
NVP15/1/1/20	20	16	0.08 \pm 0.037	125-180	1.77 \pm 0.002	2.52 \pm 0.02	0.66 \pm 0.01	0.28 \pm 0.03	2.25 \pm 0.05	36 \pm 16
NVP15/1/1/25	25	18	0.071 \pm 0.033	125-180	1.77 \pm 0.002	2.52 \pm 0.02	0.66 \pm 0.01	0.27 \pm 0.03	2.25 \pm 0.05	32 \pm 15
NVP15/1/1/30	30	22	0.17 \pm 0.068	125-180	1.77 \pm 0.002	2.52 \pm 0.02	0.66 \pm 0.01	0.26 \pm 0.03	2.25 \pm 0.05	76 \pm 30
NVP15/1/1/40	40	19	0.14 \pm 0.035	125-180	1.58 \pm 0.032	3.7 \pm 0.074	0.8 \pm 0.016	0.25 \pm 0.03	2.18 \pm 0.13	64 \pm 16
NVP15/1/1/50	50	19	0.12 \pm 0.029	125-180	1.58 \pm 0.032	3.7 \pm 0.074	0.8 \pm 0.016	0.24 \pm 0.2	2.17 \pm 0.13	55 \pm 14
NVP15/3/1/1	1	20	0.1 \pm 0.044	125-180	1.25 \pm 0.025	2.2 \pm 0.044	0.6 \pm 0.012	0.33 \pm 0.03	1.62 \pm 0.10	62 \pm 27
NVP15/3/1/10	10	21	0.19 \pm 0.061	125-180	1.25 \pm 0.025	2.2 \pm 0.044	0.6 \pm 0.012	0.30 \pm 0.03	1.72 \pm 0.10	111 \pm 36
NVP15/3/1/20	20	21	0.20 \pm 0.10	125-180	1.53 \pm 0.009	3.08 \pm 0.03	0.64 \pm 0.01	0.28 \pm 0.03	2.06 \pm 0.05	097 \pm 49
NVP15/3/1/25	25	26	0.11 \pm 0.022	125-180	1.53 \pm 0.009	3.08 \pm 0.03	0.64 \pm 0.01	0.27 \pm 0.03	2.06 \pm 0.05	53 \pm 11
NVP15/3/1/30	30	19	0.12 \pm 0.059	125-180	1.53 \pm 0.009	3.08 \pm 0.03	0.64 \pm 0.01	0.26 \pm 0.03	2.06 \pm 0.05	58 \pm 29
NVP15/3/1/40	40	21	0.19 \pm 0.065	125-180	1.29 \pm 0.026	2.6 \pm 0.052	0.6 \pm 0.012	0.25 \pm 0.03	1.78 \pm 0.11	107 \pm 37
NVP15/3/1/50	50	23	0.25 \pm 0.067	125-180	1.29 \pm 0.026	2.6 \pm 0.052	0.6 \pm 0.012	0.24 \pm 0.02	1.77 \pm 0.11	141 \pm 39
NVP15/4/1/5	5	20	0.14 \pm 0.043	125-180	1.74 \pm 0.035	4.9 \pm 0.098	1.3 \pm 0.026	0.32 \pm 0.03	2.40 \pm 0.05	58 \pm 18
NVP15/4/1/10	10	20	0.18 \pm 0.018	125-180	2.18 \pm 0.01	5.42 \pm 0.06	1.17 \pm 0.02	0.31 \pm 0.03	2.88 \pm 0.06	62 \pm 6
NVP15/4/1/15	15	17	0.3 \pm 0.051	125-180	2.02 \pm 0.01	4.96 \pm 0.04	1.16 \pm 0.01	0.29 \pm 0.03	2.74 \pm 0.06	149 \pm 44
NVP15/4/1/20	20	19	0.28 \pm 0.058	125-180	1.84 \pm 0.02	4.97 \pm 0.13	1.2 \pm 0.03	0.28 \pm 0.03	2.60 \pm 0.06	108 \pm 22
NVP15/4/1/25	25	19	0.38 \pm 0.086	125-180	2.03 \pm 0.01	4.77 \pm 0.03	1.09 \pm 0.01	0.27 \pm 0.03	2.74 \pm 0.06	138 \pm 31
NVP15/4/1/30	30	19	0.46 \pm 0.083	125-180	1.99 \pm 0.01	4.58 \pm 0.06	1.04 \pm 0.02	0.26 \pm 0.03	2.67 \pm 0.06	172 \pm 31
NVP15/4/1/35	35	19	0.44 \pm 0.085	125-180	1.95 \pm 0.02	4.82 \pm 0.04	1.02 \pm 0.01	0.26 \pm 0.03	2.66 \pm 0.06	166 \pm 32
NVP15/4/1/40	40	19	0.52 \pm 0.094	125-180	1.77 \pm 0.02	4.43 \pm 0.04	1.06 \pm 0.01	0.25 \pm 0.03	2.46 \pm 0.05	211 \pm 38
NVP15/4/1/45	45	27	0.41 \pm 0.047	125-180	1.72 \pm 0.034	4.5 \pm 0.09	1.2 \pm 0.024	0.25 \pm 0.03	2.45 \pm 0.05	168 \pm 20

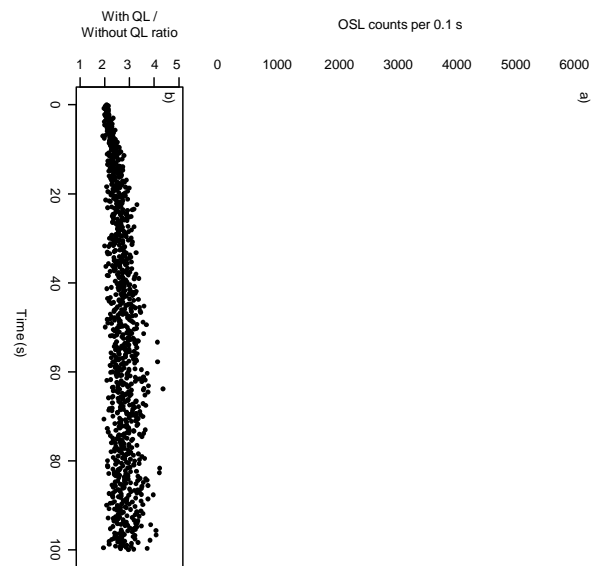


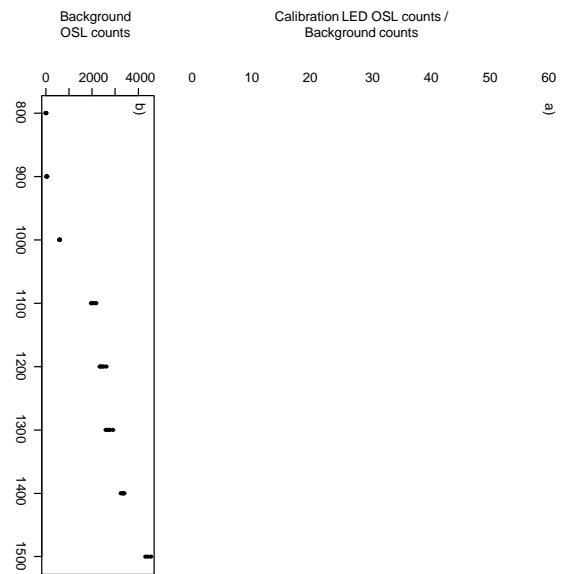


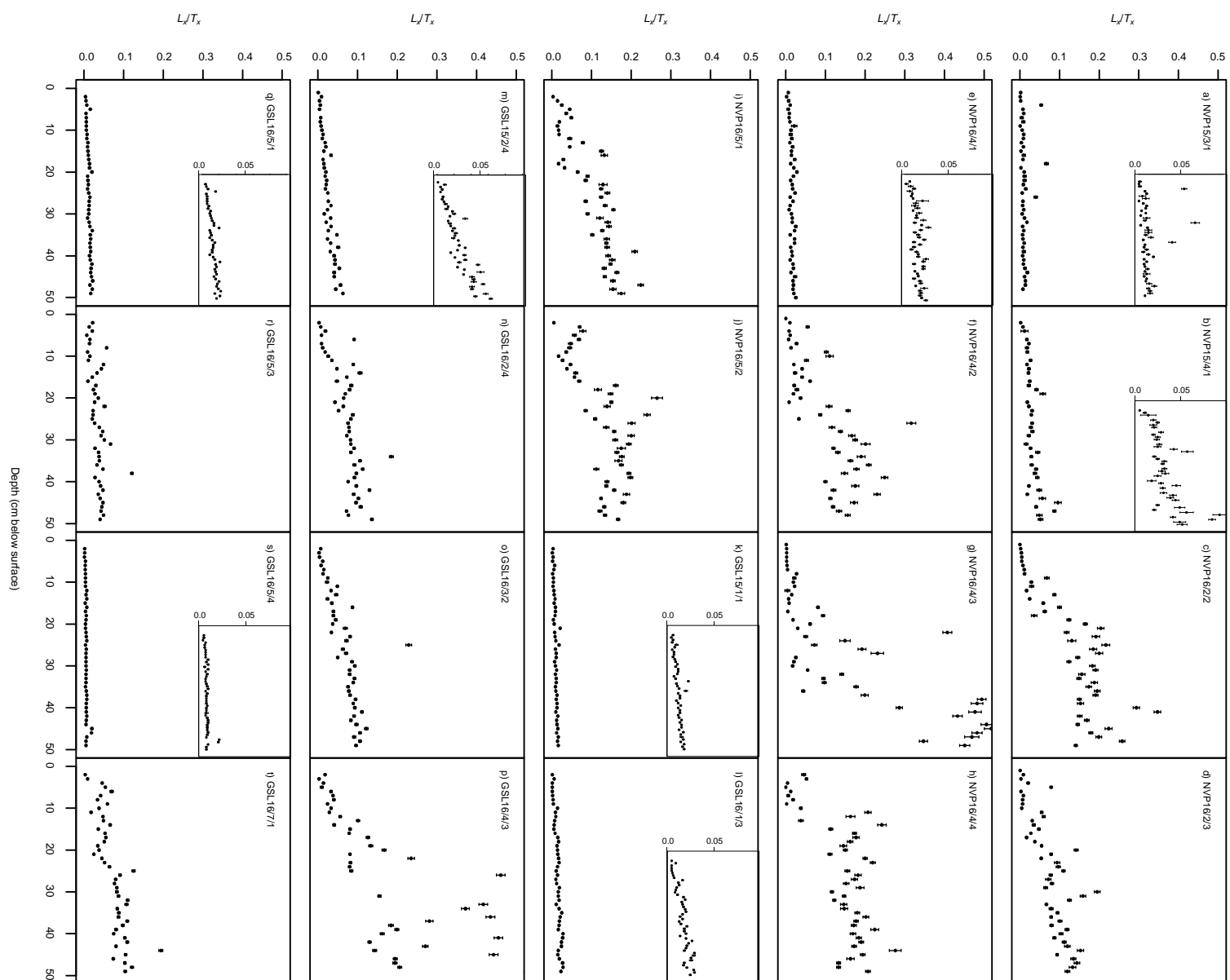


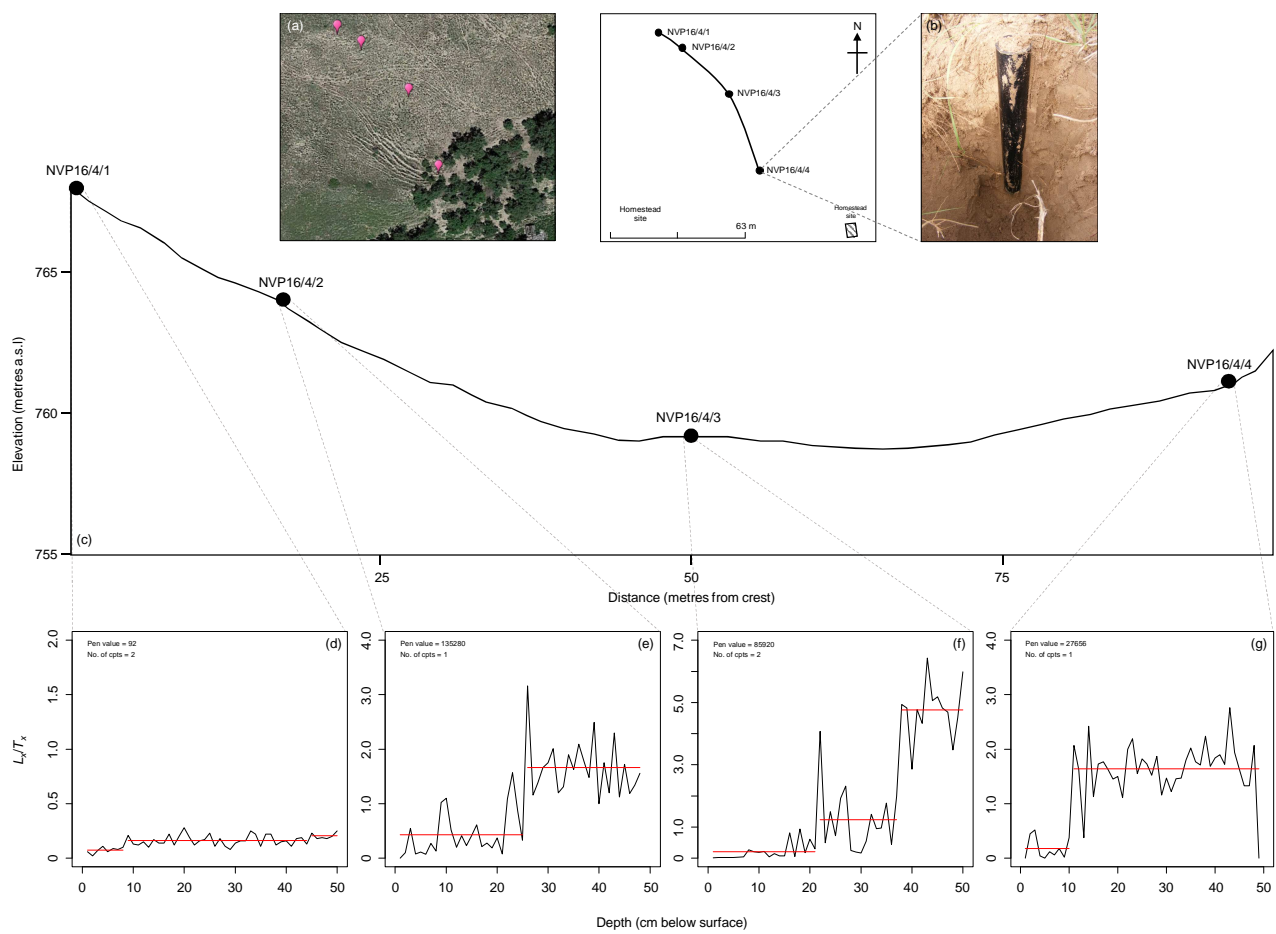


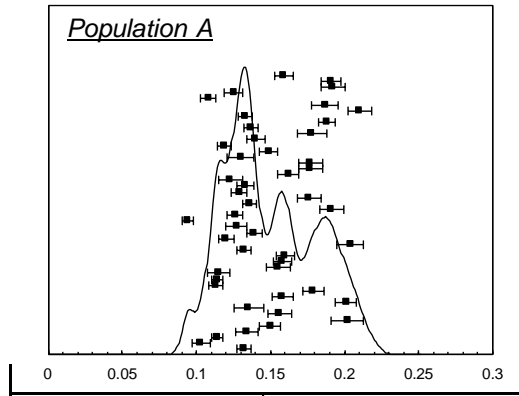










Population AAnova: Single FactorPopulation A

Mean 0.149396

Variance 0.000931

Population B

Mean 0.165128

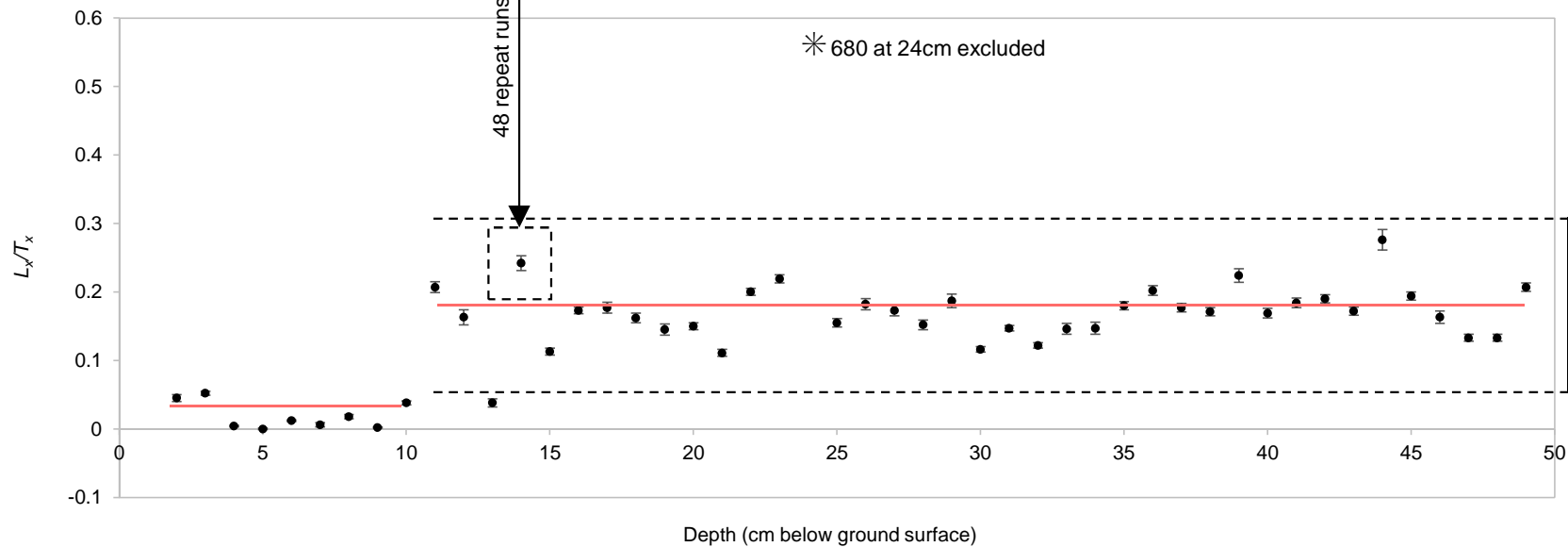
Variance 0.002111

Summary statistics

F 3.651496

F crit 3.953209

$F < F_{crit}$ and we therefore accept the null hypothesis. The means from the two populations are equal and do not show any difference.

Population B